Electronic Supplementary Material (ESI) for Nanoscale.

Supporting Information

Efficiency-Enhanced and Sidelobe-Suppressed Super-Oscillatory Lenses for Sub-Diffraction-Limit Fluorescent Imaging with Ultralong Working Distance

Wenli Li[1,2,3], Pei He[1,2,3], Weizheng Yuan[1,2,,3,], and Yiting Yu[1,2,3,*]*

1 Research & Development Institute of Northwestern Polytechnical University in Shenzhen, Room 2501, No.45, Gaoxin South 9th Road, Nanshan District, Guangdong, Shenzhen, 518057, School of Mechanical and Electronical Engineering, Northwestern Polytechnical University, Xi'an 710072, China

2 Key Laboratory of Micro/Nano Systems for Aerospace (Ministry of Education), Northwestern Polytechnical University, Xi'an 710072, China

3 Shaanxi Province Key Laboratory of Micro and Nano Electro-Mechanical Systems, Northwestern Polytechnical University, Xi'an 710072, China

** Weizheng Yuan, yuanwz@nwpu.edu.cn; Yiting Yu, yyt@nwpu.edu.cn.*

CONTENTS:

6. Simulated focusing efficiency of the SOLs

7. Experimental characterization imaging of the fluorescent particles

1. Design parameters and transmittance functions distributions of the three multiple phase-modulated SOLs

Table S1. Design parameters of the three phase-modulated SOLs

Type	**Phase levels**	**Wavelength (nm)**	**Radius/Focal length (μm)**	**Calculated Rayleigh diffraction limit**
SOL #1	0,π	532	1000/2000	0.61/0.45λ
SOL #2	0, π/2, π	532	1000/2000	0.61/0.45λ
SOL #3	0, π/2, π, 3π/2, 2π	532	1000/2000	0.61/0.45λ

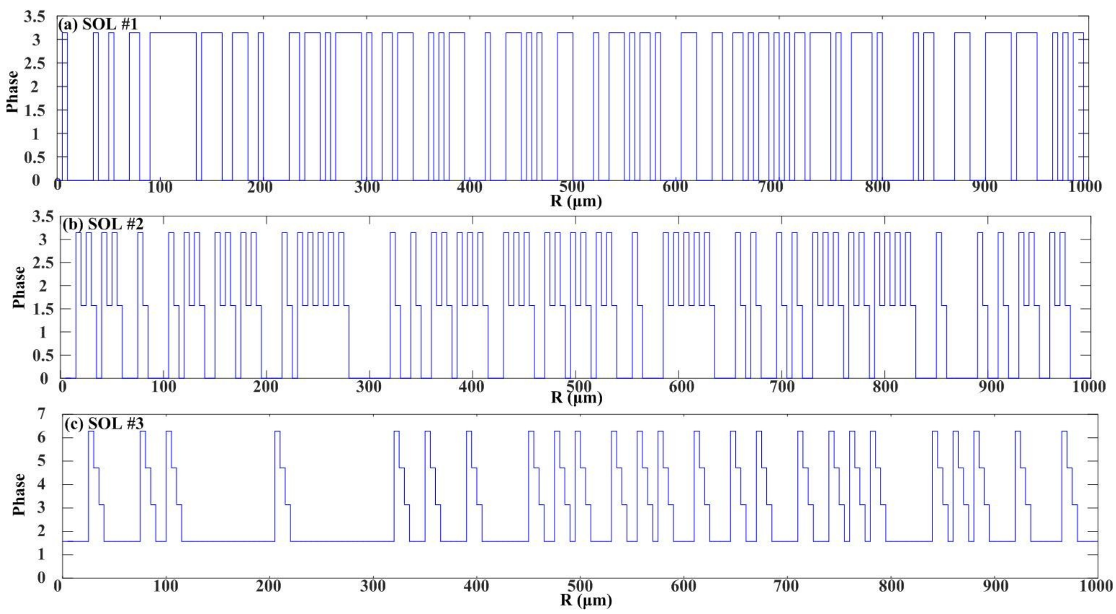

Figure S1. The transmittance functions distribution of the three optimized phase-modulation masks.

Compared with the design of traditional binary phase SOLs, the design of step-shaped SOLs based on the multiple-phase-modulated (MPM) method can be different with the several tips below:

1) The initial operation is the same as the design of traditional binary-phase SOLs, just create N random masks with (0, 1). Then just generate a constraint to obtain the two continuous "1" in the initial phase distribution.

2) Taking the stepped phase shift such as $\pi/2$, π to replace the two continuous "1" in the initial phase distribution, then the initial stepped phase distributions can be got. During the calculation of the initial optical contours in the far field, the initial stepped phase distributions are brought in.

3) After the same genetic operations performed which are kept in line with the operations in our previous design of the binary SOLs, and the above operations 1) and 2) are executed within the genetic iterations. Finally, the optimized optical distributions can be acquired after multiple genetic operations.

2. Comparison between the theoretical calculations and simulated ones

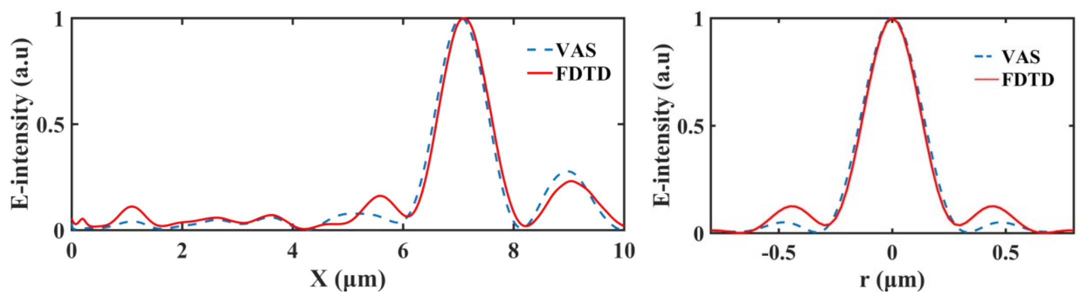

Figure S2. Comparison of the focusing performances between the VAS and FDTD for the 2-step sample R=10 μm, *f*=7 μm.

3. Influence of the shadow effect on the focusing efficiencies

Table S2. The phase level, NA, device sizes and focusing efficiency of the optimized MPM masks

Phase level	NA	Radius/μm	Focal length/μm	Focusing efficiency
0, π/2, π	0.82	10	7	11.2%
0, π/2, π	0.55	10	15	7.7%
0, π/2, π	0.45	10	20	5.0%

According to Table S2, we note that shadow effect can clearly affect the focusing efficiencies at high NA stepped SOLs. The focusing efficiencies decrease as the increase of the NA, attributing to the increased light scattering at larger diffraction angles.

4. Optical refractive index of deposited Si_xN_y layer

The optical properties of the Si_xN_y wafer deposited via plasma-enhanced chemical vapor deposition (PECVD) are measured by spectroscopic ellipsometer (ELLITOP Scientific Co., Ltd. ES01). The measured refractive index is shown in Figure S3, where detailed refractive index value at wavelength of 532 nm is n_{532}=2.25.

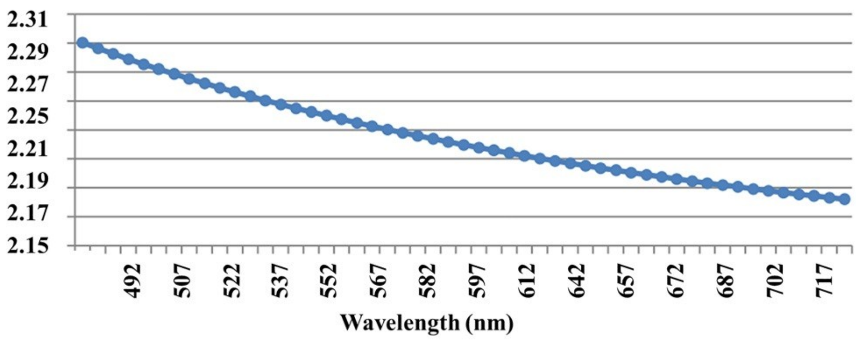

Figure S3. Experimentally measured refractive index of Si_xN_y wafer

5. Experimental characterization setup of SOLs

The experimental characterization setup is sketched in Figure S4. The individual wavelength is provided by the fiberized coupled lasers with the wavelength of 532 nm. The power for the laser can be controllable by built-in software. After collimation by a fiber coupler, the beam is directed into a customized inverted microscope (Nikon Eclipse Ti-U) using a pair of reflected mirrors and illuminates the SOLs. We used a high-magnification, high-numerical aperture objective (Nikon CFI LU Plan APO EPI 100X, NA=0.9) to collect the diffracted fields and subsequently imaged by a suitable high-resolution camera (NIKON, 2560×1280, the mesh size in the image processing software is 0.3 μm). The transverse cross-sectional distributions at specific propagation distances are obtained by z-scanning of the SOL mounted on the piezo stage (Physik Instrument, E-816). The longitudinal cross-sectional distributions are formed from built-in data processing software ImageJ.

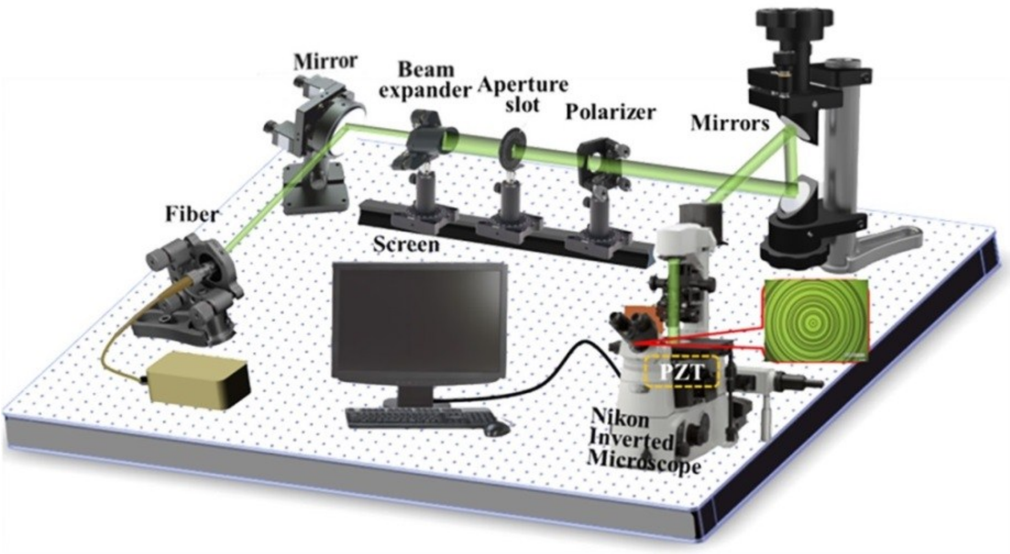

Figure S4. Schematic of optical measurement setup for SOLs' electromagnetic focusing properties. PZT: Piezoelectric Transducer.

6. Simulated focusing efficiency of the SOLs

To see the changing rules of the focusing efficiency for the three optimized phase-modulated SOLs, we just calculate the three various phase-modulated SOLs with rather small device sizes for the reason that a large-scale device simulation calculation calls for an enormous memory of the computers. The definition of the focusing efficiency for the multiple phase-modulated SOLs is the ratio of the power within a spot of diameter equal to 3 times the simulated full width at half-maximum (FWHM) to the total incident power[1]. As we can see in Table S3, the focusing efficiency of the first three SOLs is gradually improved with the increase of the phase level. Compared with the focusing efficiency of the SOL equipped with stepped phase distribution, the focusing efficiency for the SOL based on the random phase distribution seems to a little less impressive.

Table S3. The phase level, device sizes and focusing efficiency of the optimized multi-phase modulated masks

Phase level	**Radius/μm**	**Focal length/μm**	**Focusing efficiency**
0, π	10	7	3.5%
0, π/2, π	10	7	11.2%
0, π/2, π, 3π/2, 2π (Stepped phase distribution)	10	7	14.5%
0, π/2, π, 3π/2, 2π (Random phase distribution)	10	7	5.2%

7. Experimental characterization imaging of the fluorescent particles

The excitation and emission spectra curve of the fluorescent particles is shown in Figure S5, and we can see the laser source of 532 nm can be used as the incident light to stimulate the fluorescent particles. The whole imaging equipment is on the basis of the inverted fluorescent microscopy with long working distance fluorescent objective (Nikon, TU Plan Fluor 50X, NA0.8, Working distance 1 mm). The imaging samples are situated at the focal plane of the SOLs and raster scan in *x-y* plane relative to the focal spot during the imaging process by a piezo-stage (SYMC, DZNS-X200Y200Z100-01). The samples are scanned at a step size of 20 nm. The signal collection is recorded by the high-speed real-time splicing camera (Tucsen MIchrome 5 Pro) at the 35 fps with the build-in advanced imaging calculated processing software Mosaic 2.1. The 2-μm-diameter fluorescent particles are purchased from Tianjin DaE Scientific Co. Ltd.

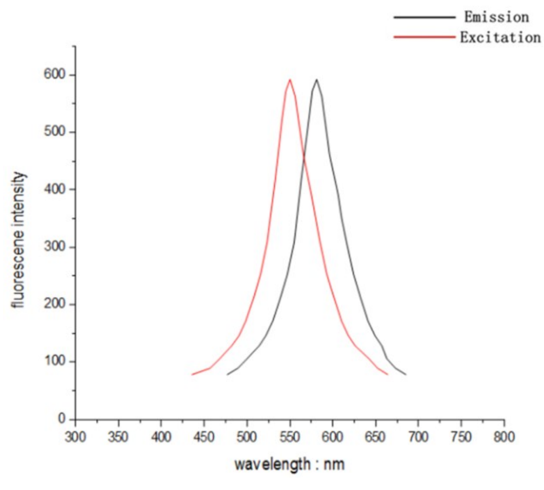

Figure S5. The excitation and emission spectra curve of the fluorescent particles.

REFERENCE

[1] Arbabi, A.; Horie, Y.; Ball, A. J.; Bagheri, M.; Faraon, Andrei. Subwavelength-thick lenses with high numerical apertures and large efficiency based on high-contrast transmitarrays. *Nat. Commun.* **2015**; 6: 7069.